The International Journal of Advanced Manufacturing Technology (2020) 107:3967–3979
https://doi.org/10.1007/s00170-020-05161-9

ORIGINAL ARTICLE

Cutting performance of micro-textured WC/Co tools in the dry cutting of Ti-6Al-4V alloy

Na Zhang[1] · Fazhan Yang[1] · Guohua Liu[1]

Received: 10 September 2019 / Accepted: 2 March 2020 / Published online: 23 April 2020

Abstract
To further improve the cutting performance of WC/Co tools in the dry cutting of Ti-6Al-4V alloy. Experiments in dry cutting titanium alloy were carried out using micro-textured YG8 tools under different cutting speeds and depths. Three kinds of YG8 tools with the rake face machined with line groove, sinusoidal groove, and rhombic groove were adopted as the micro-texture YG8 tools. The cutting force, friction coefficient of the tool-chip contact zone, chip morphology, tool wear, and surface quality of machined titanium alloy were analyzed. The results show that the micro-textured tools can effectively reduce the wear area on the rake face and flank face, improve the wear form on the rake face, reduce the occurrence of oxidation wear, and improve the surface quality of machined Ti-6Al-4V alloy. Therefore, micro-textured tools can effectively improve cutting performance and prolong tool life. The existence of micro-texture on the tool surface has a certain influence on the tool performance. The line groove-textured tool has the best effect, followed by the sinusoidal and rhombic groove-textured tools.

Keywords Textured tool · Ti-6Al-4V alloy · Laser processing · Dry cutting

1 Introduction

In the cutting process, cutting fluid can be responsible for cooling and lubrication [1, 2]. However, the application of cutting fluid for processing is facing increasing environmental pressure with the increase of the need for environmental protection [3, 4]. Dry cutting, which is nowadays considered as a popular green processing method, is becoming more and more important in production [5]. Titanium alloy is difficult-to-machine material with low elastic modulus and low thermal conductivity. Therefore, violent bond wear occurs during the process of cutting titanium alloy as lots of cutting heat is generated. As a result, the cost of machining titanium alloy is very high due to the low machining performance and short tool life [6–9].

In recent years, many scholars have proposed and proved that micro-texture machined on the tool surface can effectively improve the tribological properties between tool and chip [10, 11]. The existence of texture can improve the collection of debris and the storage of lubrication oil [12, 13]. The effect of micro-textures on gears, piston rings, bearings, computer hard disks, and cutting tools has been investigated [14–16]. It has been found that micro-texture machined on tool surface can effectively reduce tool wear, improve the surface quality of processed materials, and prolong tool life [17]. Arulkirubakaran et al. [18] found that the cutting force of vertical groove textured tool could be reduced by 30% under lubrication in comparison of a non-textured tool. Liu et al. [19] found that the textured tool can help to remove visible hard particles on the finished surface of Al_2O_3 ceramics. Hao et al. [20] fabricated a micro/nano superhydrophobic texture on a PCD diamond tool surface. The experiment of cutting titanium alloy under micro-lubrication was carried out, and the friction mechanism of textured tools was explored. Sanjib et al. [21] reported that the texture can improve the tribological

✉ Fazhan Yang
fazhany@163.com

Na Zhang
1182984075@qq.com

[1] School of Mechanical & Automotive Engineering, Qingdao University of Technology, 777 Jialingjiang East Road, Huangdao District, Qingdao City, Shandong Province, China

characteristics of the rake face and chip contact zone of machined alloy and improve tool life. It is found that the kind of texture has a great influence on the cutting performance of micro-textured tools. Xing et al. [22] found that the wavy textured tool showed lower cutting force and cutting temperature than the line textured tool and non-textured tool. Orra et al. [23] found that the effect of vertical line texture samples was the best, and the friction coefficient of non-texture samples could be decreased by 11.9%. Chen et al. [24] found that the texture tool can effectively improve the cutting performance of the milling tool, and the line groove texture specimen parallel to the main cutting edge is more effective to reduce the length of drilling chips and the tearing phenomenon of the cutting surface.

It is found that the micro-texture on the WC/Co tool surface can effectively improve the cutting performance in cutting titanium alloy. Mishra et al. [25] found that the existence of a coat and texture on the tool surface could reduce the tool-chip contact length and its cutting force effectively. Li et al. [26] indicated that the existence of a texture did not make a difference of the tool strength but could effectively improve the cutting performance. Arulkirubakaran et al. [27] indicated that the textured tool can reduce the frictional temperature and cutting force in processing effectively. Although a few works have been carried out, the wear mechanism on the tool-workpiece interface and chip morphology of tools needs to be further studied in the dry cutting process of cemented carbide.

In this study, line, sinusoidal, and rhombic rake-faced textures were manufactured on the rake face of YG8 tool. Experiments in dry cutting titanium alloy were carried out. The cutting force, friction coefficient between the tool rake face and chips, chip morphology, tool wear, and machined surface quality of processed titanium alloy were researched.

2 Experimental details

2.1 Sample treatment

Ti-6Al-4V alloy bars (Dongguan Copper Titanium Material Co., Ltd.), with size of Φ100 mm × 150 mm, were selected as the experimental materials. The properties of the titanium alloy material are shown in Table 1. The YG8 cemented carbide blade of 4,160,511 (Zhuzhou Diamond Cutting Tool Co., Ltd.) was selected as the experimental tool. The morphology of the tool is displayed in Fig. 1. The properties of the YG8 tool material are shown in Table 2. Carbide tools were washed with an ultrasonic cleaning machine. Using YLPN-1-100-200-R optical fiber laser processing equipment, three kinds of groove textures, line, sinusoidal (standard sine curve), and rhombic (rhombic line with 90° angle), with groove spacing of 50 μm, were machined in the range of 5 mm × 5 mm on the rake face of YG8 tool. The wavelength, pulse width, frequency, power, scanning speed, and repeat number of the fiber laser were 1064 nm, 10 ns, 20 kHz, 40 W, 100 mm/s, and 200 times, respectively. After the texture processing of the cemented carbide surface was completed, 2000-mesh sandpaper was used to grind the texture surface, and polishing and then ultrasonic cleaning were carried out. The two-dimensional morphology on the YG8 tool rake face was observed by scanning electron microscopy (SEM, Hitahi Company), as shown in Fig. 2. The three-dimensional texture morphology, observed by an optical 3D surface profiler (Super View W1, China Map Instrument Co., Ltd.), is shown in Fig. 3. The width and depth of the three kinds of groove textures are 103.120 μm and 10.550 μm, respectively.

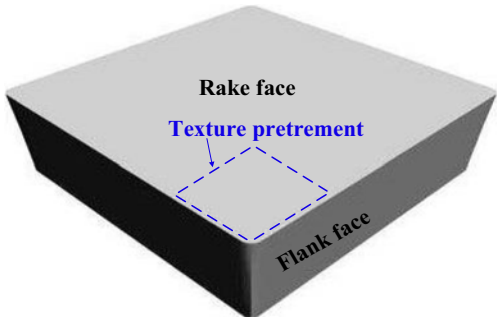

Fig. 1 The morphology of the YG8 tool

The prepared sample included the following: non-textured tool specimens (SS), line groove-textured specimens (LG), sinusoidal groove-textured specimens (SG), and rhombic groove-textured specimens (RG).

Table 1 Properties of the Ti-6Al-4V alloy material

Components (wt%)	Density (g/cm^3)	Hardness (HRA)	Thermal conductivity (W/m·k)	Coefficient of thermal expansion ($\times 10^{-6}$/k)
Ti + 6%Al + 4%V	4.44	68	5.44	8.53

2.2 Experimental setting

Dry cutting experiments of YG8 tools were carried out on the lathe-equipped CA6140. The experimental settings are shown in Fig. 4. Titanium alloy bars are mounted on chucks. The cemented carbide tool is mounted on a tool holder. The geometric parameters of the tool installation are shown in Table 3. The cutting parameters are shown in Table 4, and the cutting force is measured by a three-

Table 2 Properties of the YG8 tool material

Components (wt%)	Density (g/cm^3)	Hardness (HRA)	Bending strength (MPa)	Modulus of elasticity (GPa)	Thermal conductivity (W/m·k)
WC + 8%Co	14.6	89	1840	630	79.6

dimensional cutting force diagram during the cutting processing, as shown in Fig. 5.

The cutting force is followed by YDC-III 89A three-directional piezoelectric turning dynamometer (designed by Dalian University of Technology). The chip micro-morphology and tool wear morphology were observed by S-3400N scanning electron microscopy (Hitahi Company). The element composition of the tool wear surface was measured by an EMAX X-atc electric refrigeration X-ray spectrometer (Hitahi Company). The surface quality of the processed Ti-6Al-4V alloys was measured by a TIME3220 surface roughness instrument (Beijing Time Group Company).

3 Results

3.1 Cutting forces

The cutting forces produced by the YG8 tools in dry cutting titanium alloy are shown in Fig. 6 ($a_p = 0.3$ mm). The main cutting force of the tools is displayed in Fig. 6a. The feed force of the tools is displayed in Fig. 6b. Figure 6 shows the cutting forces of non-textured tools (SS) and three kinds of textured tools (LG, SG, RG) decrease at different turning speeds. Under the same conditions, the cutting forces of line, sinusoidal, and rhombic textured tools are always less than those of non-textured tools. Among the three textured tools, the line groove-textured tool shows the least cutting force in comparison of sinusoidal and rhombic groove-textured tools. The main cutting force of the line, sinusoidal, and rhombic groove-textured tools at the cutting speed of 47.7 m/min, compared with the non-textured tool, decreases by 29.2%, 13.6%, and 5%, respectively, and the feed force decreases by 32.8%, 10.8%, and 4%, respectively.

Figure 7 shows the cutting force produced by non-textured and textured tools in dry cutting titanium alloys at different turning depths ($v = 47.7$ m/min). The main cutting force of the tools is displayed in Fig. 7a. The feed force of the tools is displayed in Fig. 7b. When the cutting depth increases, the cutting forces of both the non-textured and textured tools increase greatly. The cutting forces of the three kinds of textured tools are always less than those of the non-textured tools regardless of turning depths. The main cutting force of the line, sinusoidal, and rhombic-textured tools, compared with the

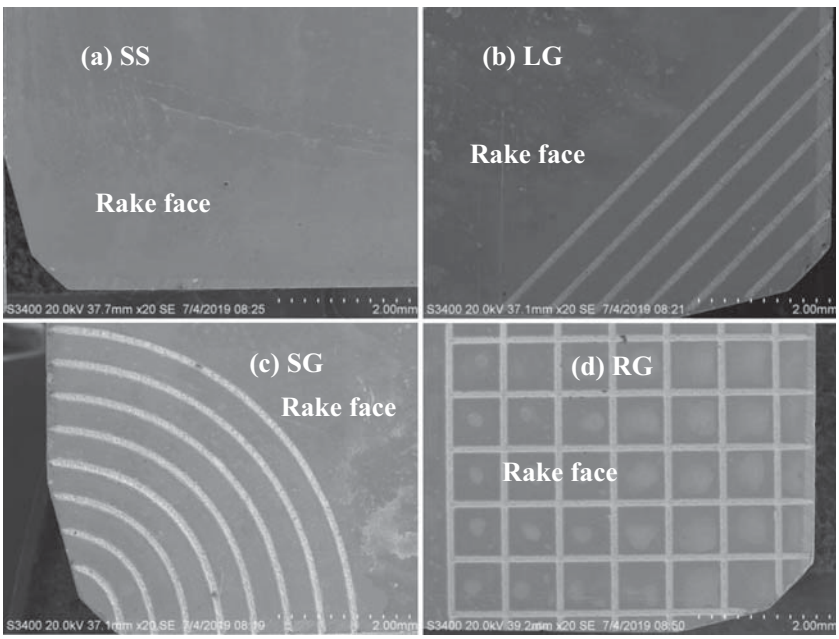

Fig. 2 Two-dimensional morphology of the non-textured tool and textured tools

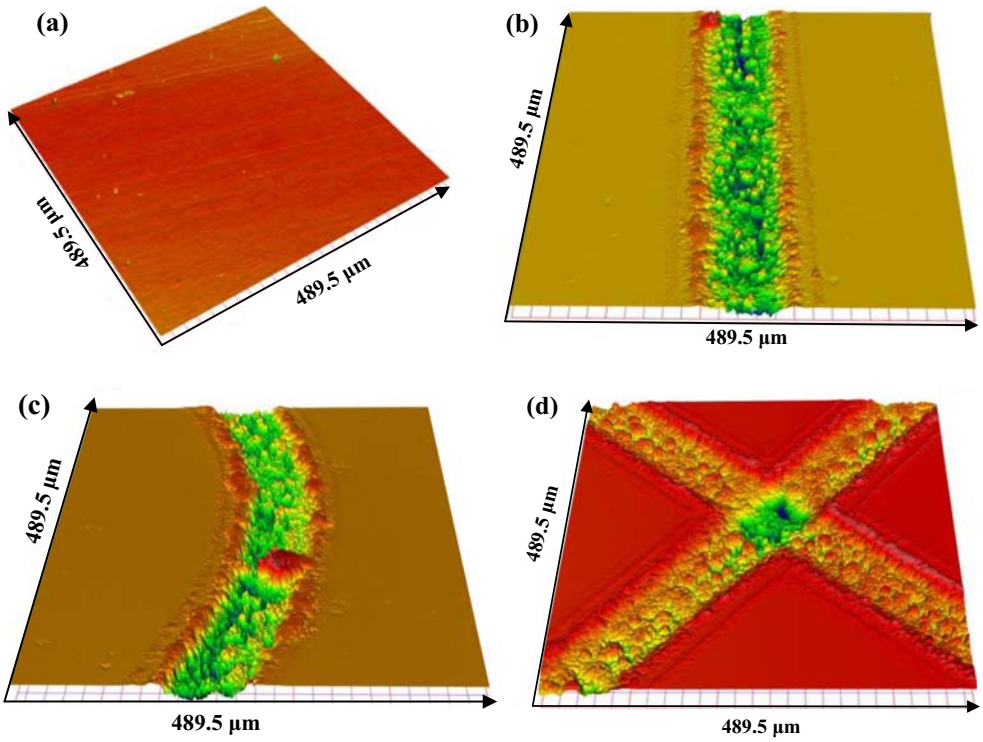

Fig. 3 Three-dimensional morphology of the non-textured tool and textured tools: **a** non-textured tool SS; **b** line-textured tool LG; **c** sinusoidal-textured tool SG; **d** rhombic-textured tool RG

non-textured tool at the cutting depth of 0.4 mm, is reduced by 24.8%, 10.7%, and 3.6%, respectively, and the feed force is reduced by 40.5%, 22.8%, and 1.6%, respectively.

In the experiments involving different cutting speeds and depths, the influence of cutting depth on cutting forces is more significant than cutting speed. It is found that, under different experimental conditions, textured tools exhibit less cutting forces than non-textured tools. The line groove-textured YG8 tool always shows the least cutting forces, followed by the sinusoidal and rhombic-textured YG8 tools. Compared with the sinusoidal and rhombic-textured YG8 tools, the effect of the line-textured YG8 tool is more significant ($v = 47.7$ m/min, $a_p = 0.2$ mm). The main cutting force of the line-textured YG8 tool decreases by 36.7%, and the feed force decreases by 42.4%, compared with the non-textured tool.

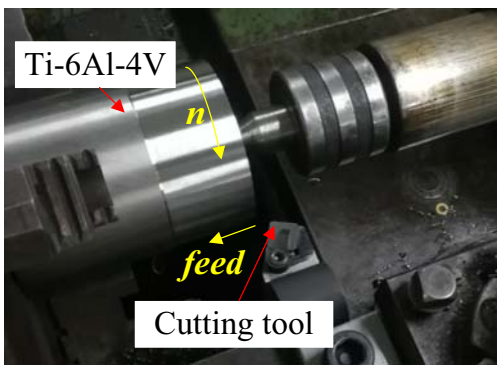

Fig. 4 Cutting experimental setup

3.2 Friction coefficient between the YG8 tool's rake face and workpiece

In the cutting process, ignoring the force acting on the tool flank face, the average friction coefficient between the YG8 tool rake face, and workpiece can be approximately calculated by Eq. (1) [28, 29]:

$$\mu = \tan\beta = \tan\left[\gamma_0 + \arctan\left(\frac{F_y}{F_z}\right)\right] \tag{1}$$

where β represents the friction angle of the tool, γ_0 represents the rake angle, F_z represents the main cutting force, and F_y represents the axial thrust force.

Figures 8 and 9 show the average friction coefficients between tool rake face and workpiece at different turning speeds and depths, respectively. In Fig. 8, when the cutting speed increases, the friction coefficient between the rake face of non-textured and textured tools and workpiece increases, and the friction coefficient of the non-textured tools is always larger than that of the textured tools. The line groove-textured tool exhibits the smallest friction coefficient, and when the turning speed is 71.9 mm/s, the friction coefficient decreases by 10%, compared with the non-textured tool. The variation trend shown in Fig. 9 is similar to that in Fig. 8. The line groove-textured YG8 tools

Table 3 The geometric angles of the tool

Nominal angles	Rake angle γ_o	Clearance angle α_o	Inclination angle λ_s	Side cutting edge angle κ_r
Angle	6°	11°	− 6°	75°

exhibit the minimum friction coefficient, followed by the sinusoidal-textured YG8 tools and rhombic-textured YG8 tools. The friction coefficient of the tools increases greatly when the cutting depth increase. In the process of increasing the cutting depth from 0.1 to 0.4 mm, the friction coefficient of the non-textured tools, line-textured tools, sinusoidal-textured tools, and rhombic-textured tools increases by 38%, 31%, 40%, and 48%, respectively.

3.3 Chip morphology

The macro-morphology of the chips produced by four kinds of tools in cutting titanium alloys is shown in Fig. 10. The curling radius of the textured tools decreases with respect to the non-textured YG8 tool, while the chip of the line-textured YG8 tool decreases by 50.4% compared to the non-textured tool.

Figures 11 and 12 show the micro-morphology of the chips produced by the different kinds of tools. Figure 11 shows the free surface morphology of the chips, and Fig. 12 shows the morphology of the back surface of the chips. The chip morphology produced by the non-textured tool is more irregular which shows violent serrated shape, and the back surface of the chip is attached with an adhesive. The chip morphology of the textured tools is smooth, the free surface of the chips is less bonded, there is no bulk bond on the back surface of the chips.

Table 4 The experimental cutting parameters

Kinds of tool	Cutting speed v (m/min)	Cutting depth a_p (mm)	Feed rate f (mm/r)	Cutting time (s)
Non-textured tool	22.7	0.3		
	47.7	0.3		
Line-textured tool	71.9	0.3		
Sinusoidal-textured tool	90.4	0.3	0.2	160
	47.7	0.1		
Rhombic-textured tool	47.7	0.2		
	47.7	0.3		
	47.7	0.4		

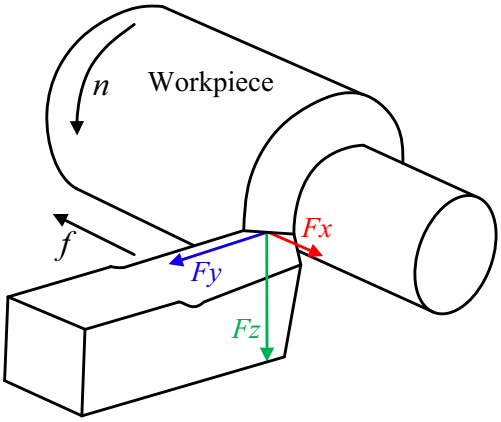

Fig. 5 Sketch of three cutting force directions of the cutting tool. **a** Main cutting force. **b** Feed force

3.4 Wear on the tools' rake face

Figure 13 demonstrates the wear morphology and element distribution on the rake face of the non-textured tool (v = 90.4 m/min, a_p = 0.4 mm). Figure 13 a shows that a crescent depression wear occurs near the main cutting edge on the rake face of the non-textured tool (SS), a certain thickness of the bonding layer occurs near the secondary cutting edge, and a larger area of bonding occurs on the rake face. Figure 13 b is an enlarged image of region A. Figure 12 c, d, and e are EDX energy spectrum analyses of regions B, C, and D, respectively. There are a lot of Ti elements and some O elements in region B, as well as Ti elements, in region C. In addition to 57% Ti element, a large number of W and C elements were found in region C.

Figures 14, 15, and 16 show the wear morphology and element distribution on rake face of the line, sinusoidal, and rhombic-textured tools, respectively (v = 90.4 m/min, a_p = 0.4 mm). From the wear morphologies on the rake faces, displayed in Figs. 14a; 15a; and 16a, it can be indicated that the wear area of the groove textured tools is significantly reduced in contrast with the non-textured tool, and the grooved textures near the main cutting edge are covered by bonds. The wear width of the textured YG8 tools is smaller than that of the non-textured YG8 tool. Layered bonding occurs at the cutting edge on the rake face. From the EDX element distribution of the wear area on the rake face of the textured tools, shown in Figs. 14c, d; 15c, d; and 16c, d, it can be seen that there are a lot of Ti elements in the wear area near the main cutting edge and in the grooved textures on the rake face of the textured tools, as well as a few W elements in the grooved textures of the textured tools. In addition, there are some O elements in the wear area and grooved textures of the rhombic tool, as shown in Fig. 16 c and d.

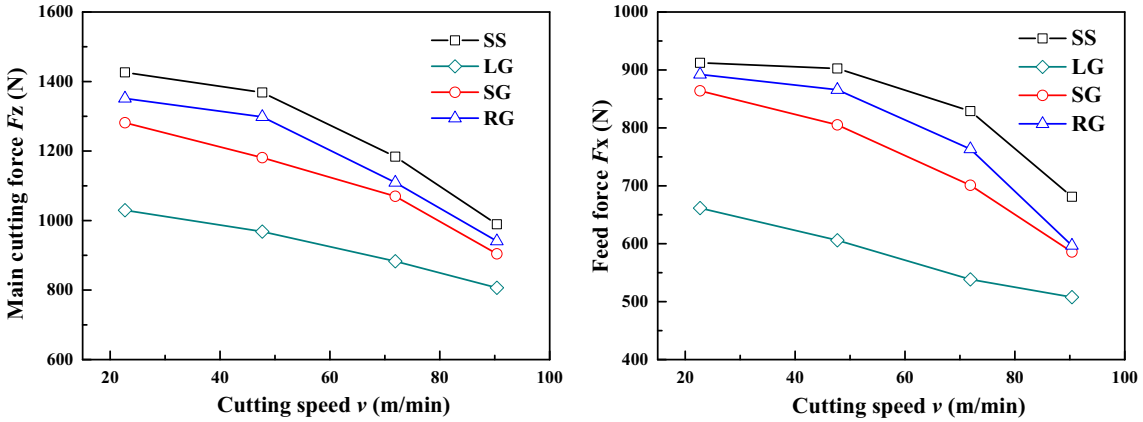

(a) Main cutting force. (b) Feed force.

Fig. 6 Cutting forces of the tools at different cutting speeds ($a_p = 0.3$ mm). **a** Main cutting force. **b** Feed force

3.5 Wear on the tools' flank face

Figure 17 demonstrates the wear morphology on the flank face of the non-textured tool and textured tools from cutting titanium alloys. The wear area on the flank face of the non-textured tool is large, and a thicker bonding layer is formed at the tool tip as demonstrated in Fig. 17a. In Fig. 17 b, c, and d, the wear area of the line, sinusoidal, and rhombic-textured tools is smaller in comparison of the non-textured tool, and the wear area of the line-textured tool is the smallest.

3.6 Machined surface roughness of Ti-6Al-4V alloy

Figure 18 shows the surface roughness of the titanium alloy machined with four kinds of YG8 tools ($v = 90.4$ m/min, $a_p = 0.4$ mm). Figure 18 shows that the surface roughness of the titanium alloy processed by three kinds of textured tools is reduced in comparison with that of the alloy processed by the non-textured tool. The surface quality of the Ti-6Al-4V alloy processed by the line-textured tool is the best, and the surface roughness of the Ti-6Al-4V alloy processed by the line-textured tool is 26.7% lower than that of the alloy processed by the non-textured YG8 tool. The surface roughness of the titanium alloy machined by the sinusoidal- and rhombic-textured tools is reduced by 17.6% and 4.2%, compared with that of the alloy machined by the non-textured tool.

4 Discussion

The grooved textures were machined on the YG8 tool's rake face to cut titanium alloy. A cutting schematic diagram is

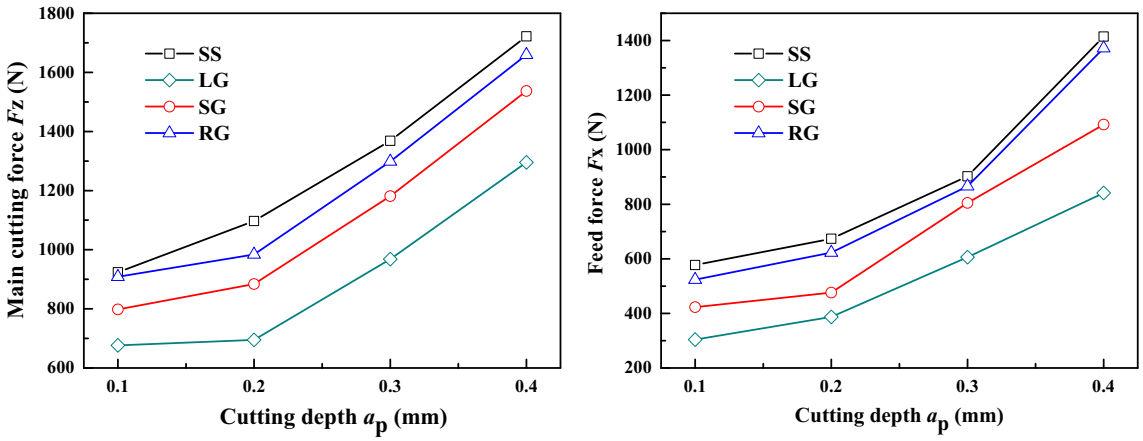

(a) Main cutting force. (b) Feed force.

Fig. 7 Cutting forces of the tools at different cutting depths ($v = 47.7$ m/min)

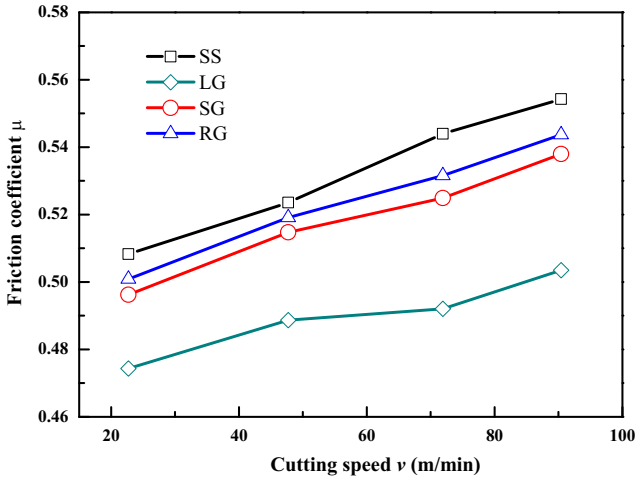

Fig. 8 Friction coefficient in the tool–chip contact area on the rake face at different cutting speeds ($a_p = 0.3$ mm)

shown in Fig. 19. The contact length of the chips of the non-textured tool is l_f, and the contact length of the chips of the textured tool is l_f', which can be calculated by Eq. (2) [30]:

$$l_f' = l_f - nd \tag{2}$$

where n represents the number of textures in the tool-chip interface of a tool, and D represents the groove diameter of a single texture.

The existence of a texture reduces the tool-chip contact length and tool-chip contact area. The results show that the curl radius of the three kinds of textured tools is smaller than that of the non-textured tool, as shown in Fig. 8.

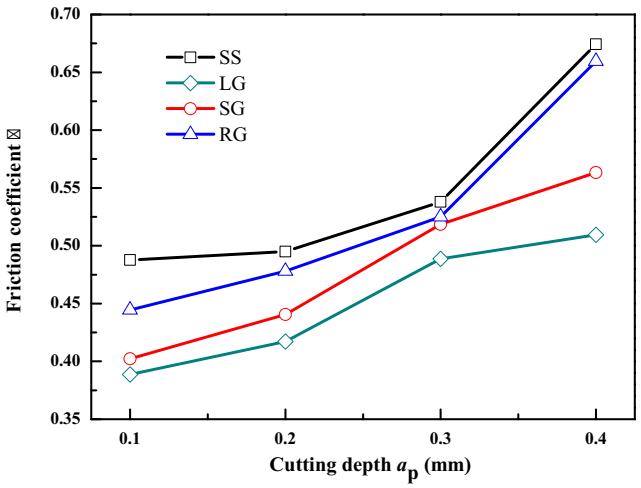

Fig. 9 Friction coefficient in the tool–chip contact area on the rake face at different cutting depths ($v = 47.7$ m/min)

The cutting force of the tool can be approximately calculated by the following Eq. (3) and Eq. (4) [31–33]:

$$F_z = a_w l_f \tau_c \left(\sin\gamma_0 + \frac{\cos\gamma_0}{\tan\beta} \right) \tag{3}$$

$$F_x = a_w l_f \tau_c \left(\cos\gamma_0 - \frac{\sin\gamma_0}{\tan\beta} \right) \cos(\varphi_r + \varphi_\lambda) \tag{4}$$

where a_w represents the cutting width, l_f represents the tool–chip contact length on the rake face, τ_c represents the average sheer force, γ_0 represents the rake angle of the tool, β represents the friction angle, φ_r represents the residual deviation angle, and φ_λ represents the chip outflow angle.

The contact length l_f' of the textured tools is smaller than that of the non-textured tool, so the cutting forces are reduced. As demonstrated in Figs. 6 and 7, the cutting forces of the textured tools are always smaller than those of the non-textured tools, while the line-textured tools show the minimum cutting force, relative to the sinusoidal and rhombic-textured tools.

In the turning process with the cemented carbide tool, because of the poor thermal conductivity and small elastic modulus of the titanium alloy material, the cutting heat cannot be discharged in time, and a concentrated high temperature zone is formed. Crater wear is formed on the rake face of the non-textured tool, as displayed in Fig. 13b. In Fig. 13a, the bonding condition on the rake face is more serious. Layered bonding is distributed over a large area. Crater wear is formed near the main cutting edge. Crater wear reduces the strength of the cutting edge and easily leads to cutting edge damage. An EDX element distribution in the crater wear of the non-textured tool (region B in Fig. 13b), which contains a large amount of Ti elements and a small amount of C, Al, and V elements, is shown in Fig. 13c. It can be inferred that region B in Fig. 13a is a titanium alloy bond, where the bond wear occurs. The composition of region C (Fig. 13b) is shown in Fig. 13d. In addition to Ti, C, Al, and V elements in the titanium alloy materials, there is a small amount of O elements. Compared with region B (Fig. 13b), it can be inferred that, besides the bonding wear, Ti and O in the air react at a high temperature to form titanium oxide, which results in oxidative wear. Region D in Fig. 13b is shown in Fig. 13e, which contains Ti, C, Al, and V elements, as well as Co and W elements. In addition, the content of C elements in this region is also higher than that in region B, as shown in Fig. 10b. YG8-cemented carbide is composed of 92% WC and 8% Co. It can be inferred that the bonds in area D (Fig. 13b) are exfoliated with the wear on the

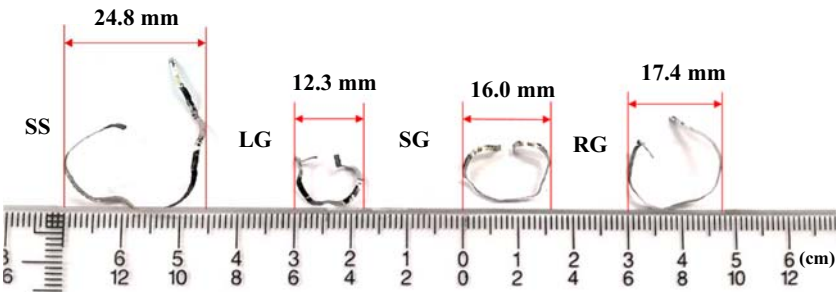

Fig. 10 Chip macro-morphology of the non-textured and textured tools ($v = 90.4$ m/min, $a_p = 0.4$ mm)

rake face, exposing the YG8 material matrix. Therefore, bond wear and diffusion wear occur in region D.

Figures 14b; 15b; and 16b show that the wear width where near the main cutting edge on the textured tools' rake face decreases with respect to the non-textured tool. The wear width of the rhombic-textured tool is 204 μm, which is 34% less than the non-textured tool. The EDX element distribution of region B is indicated in Figs. 14b and 15b. The EDX element distribution of region B in the wear area of the line- and sinusoidal-textured tools is displayed in Figs. 14c and 15c, respectively. The area is mainly covered by Ti, C, Al, and V elements, resulting in a bond wear of the titanium alloy. The main element in the grooves is Ti, which indicates that the texture near the main cutting edge has been completely covered by debris, as indicated in Figs. 14d and 15d.

The EDX element analysis of regions B and C is displayed in Fig. 16b. The EDX element analysis of region B of the rhombic-textured tool is shown in Fig. 16 c and d. Regions B and C contain Ti, C, Al, V elements and some O elements. It can be inferred that bond wear and partial oxidation wear occur in this region.

In addition, the wear near the main and minor cutting edges, and away from the cutting edges of the non-textured tool, is serious in Fig. 13a. The wear on the textured tools' rake face occurs at the main and minor cutting edges, and only a small amount of debris is bonded away from the cutting edges.

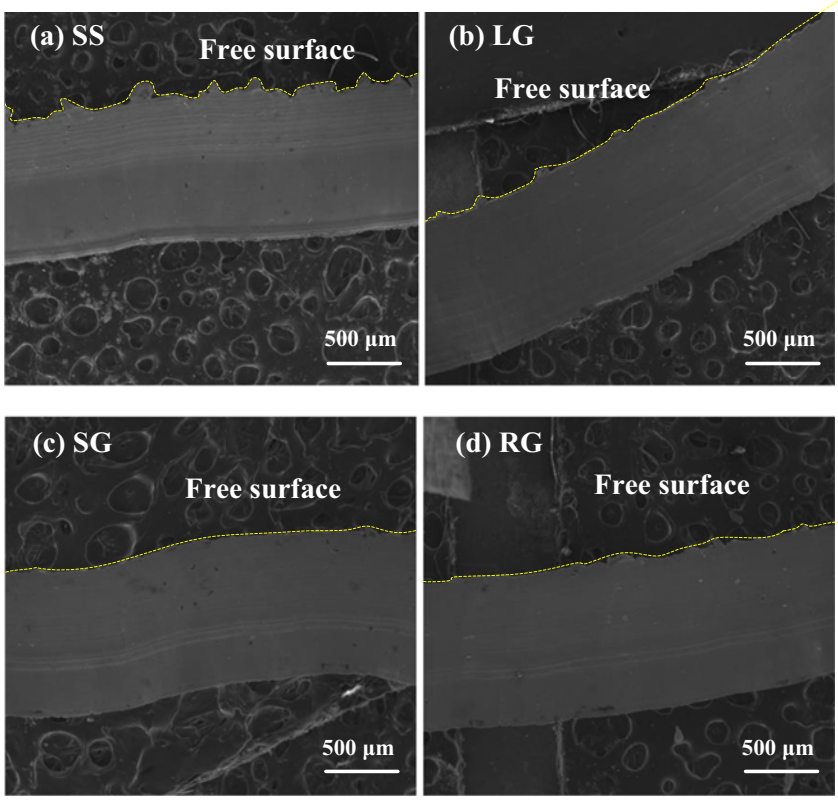

Fig. 11 SEM of the free surface of the chips ($v = 90.4$ m/min, $a_p = 0.4$ mm)

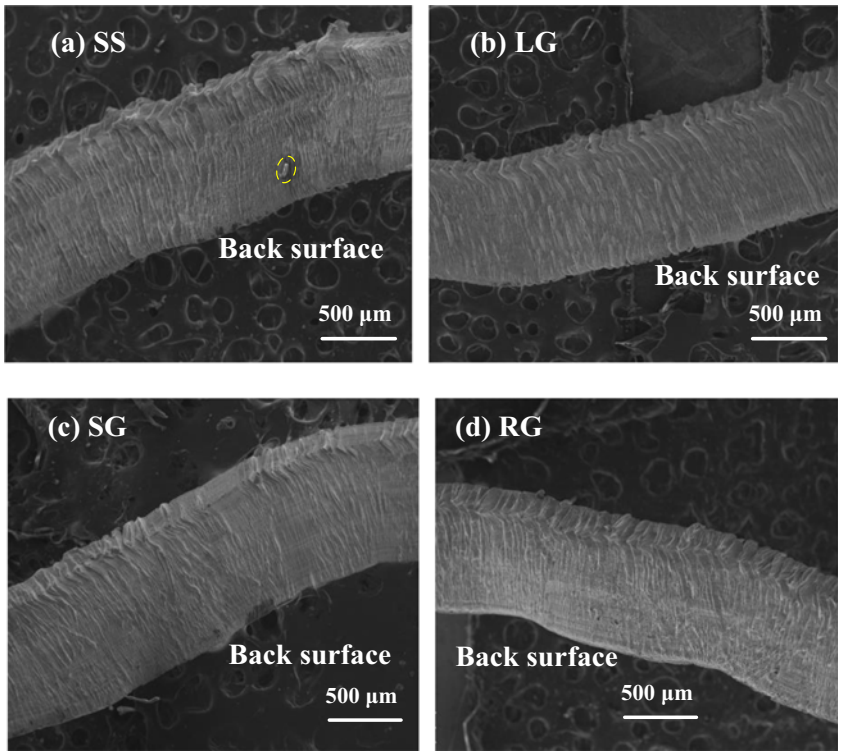

Fig. 12 SEM of the back surface of the chips (v = 90.4 m/min, a_p = 0.4 mm)

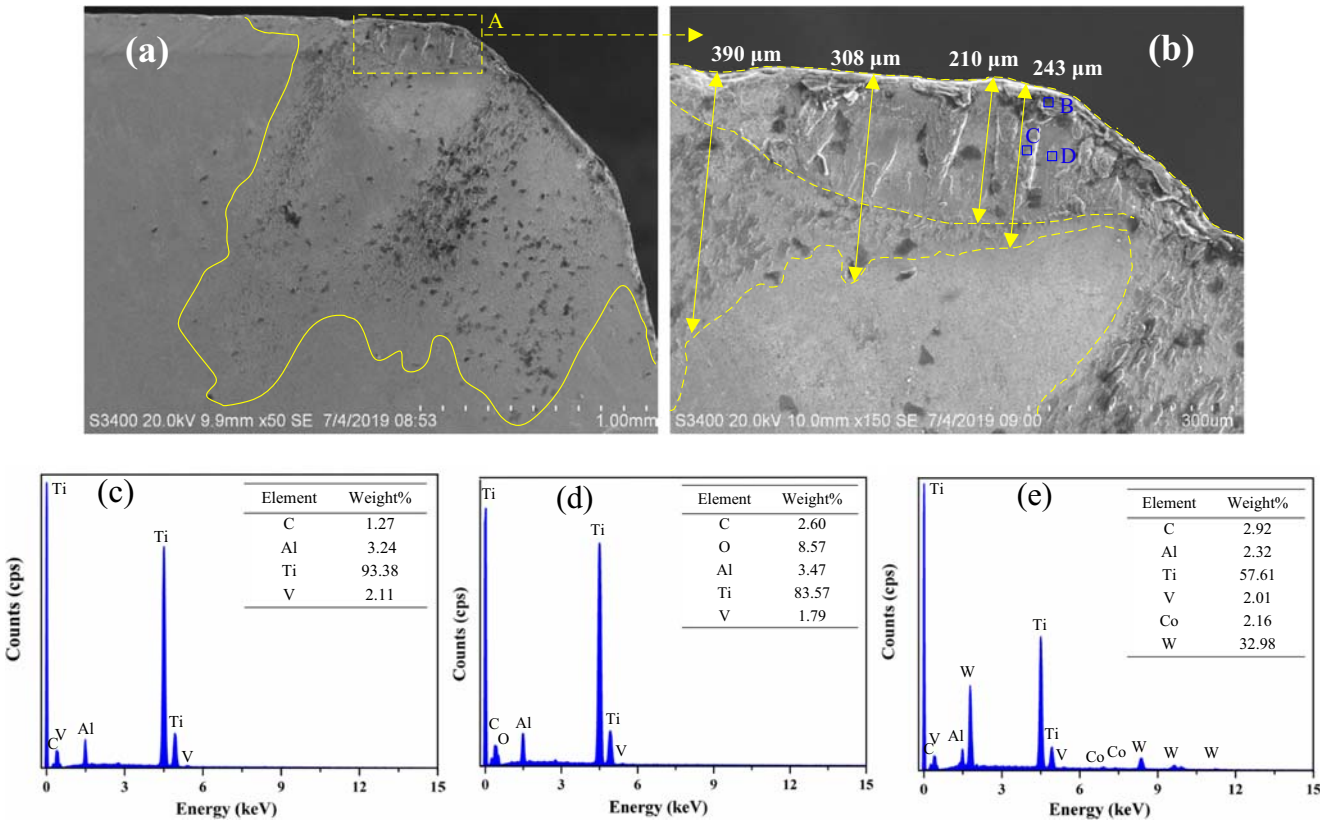

Fig. 13 SEM and EDX of the wear on the rake face of the non-textured tool (v = 90.4 m/min, a_p = 0.4 mm): **b** enlarged view of A; **c** EDX of B; **d** EDX of C; **e** EDX of D

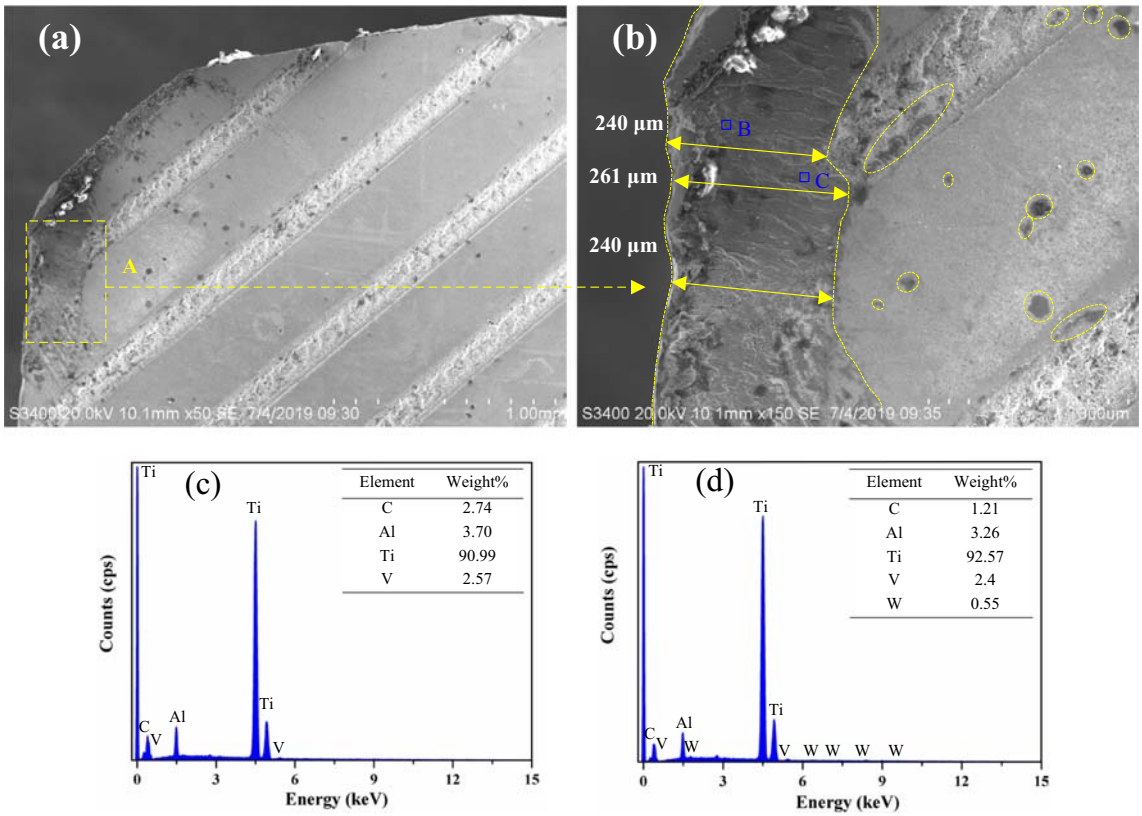

Fig. 14 SEM and EDX of the wear on the rake face of the line-textured tool ($v = 90.4$ m/min, $a_p = 0.4$ mm): **b** enlarged view of A; **c** EDX of B; **d** EDX of C

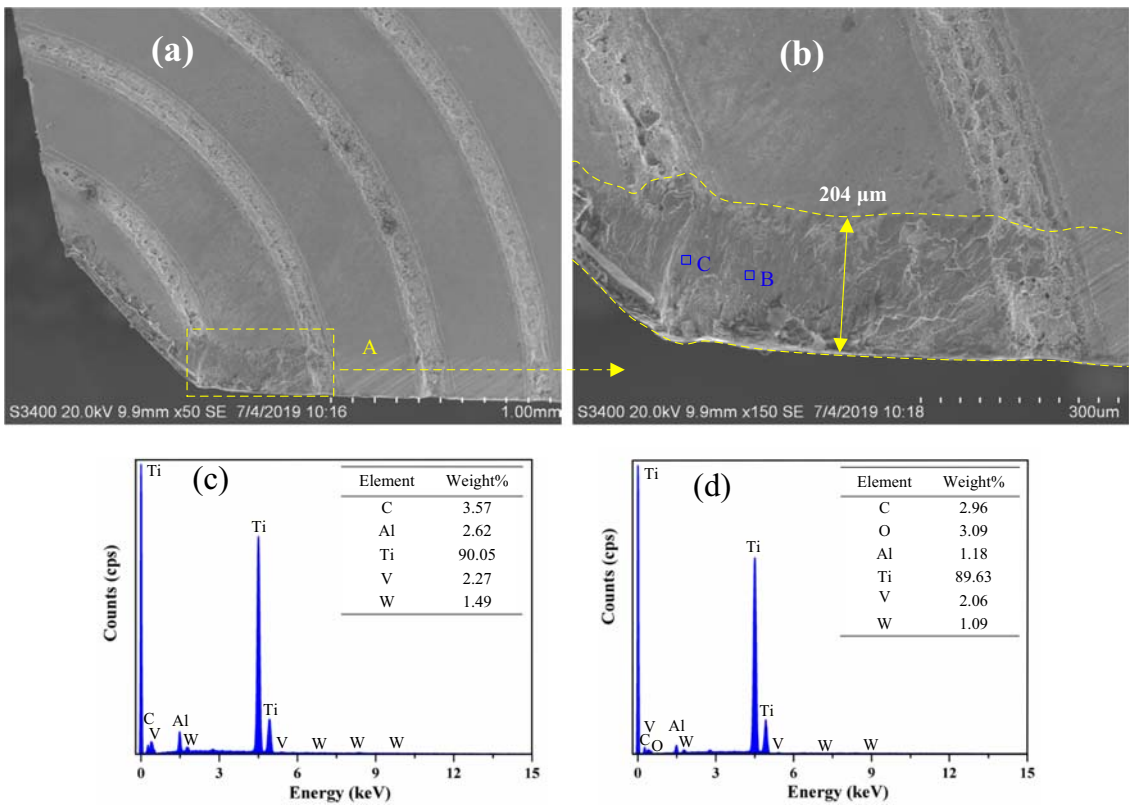

Fig. 15 SEM and EDX of the wear on the rake face of the sinusoidal-textured tool ($v = 90.4$ m/min, $a_p = 0.4$ mm): **b** enlarged view of A; **c** EDX of B; **d** EDX of C

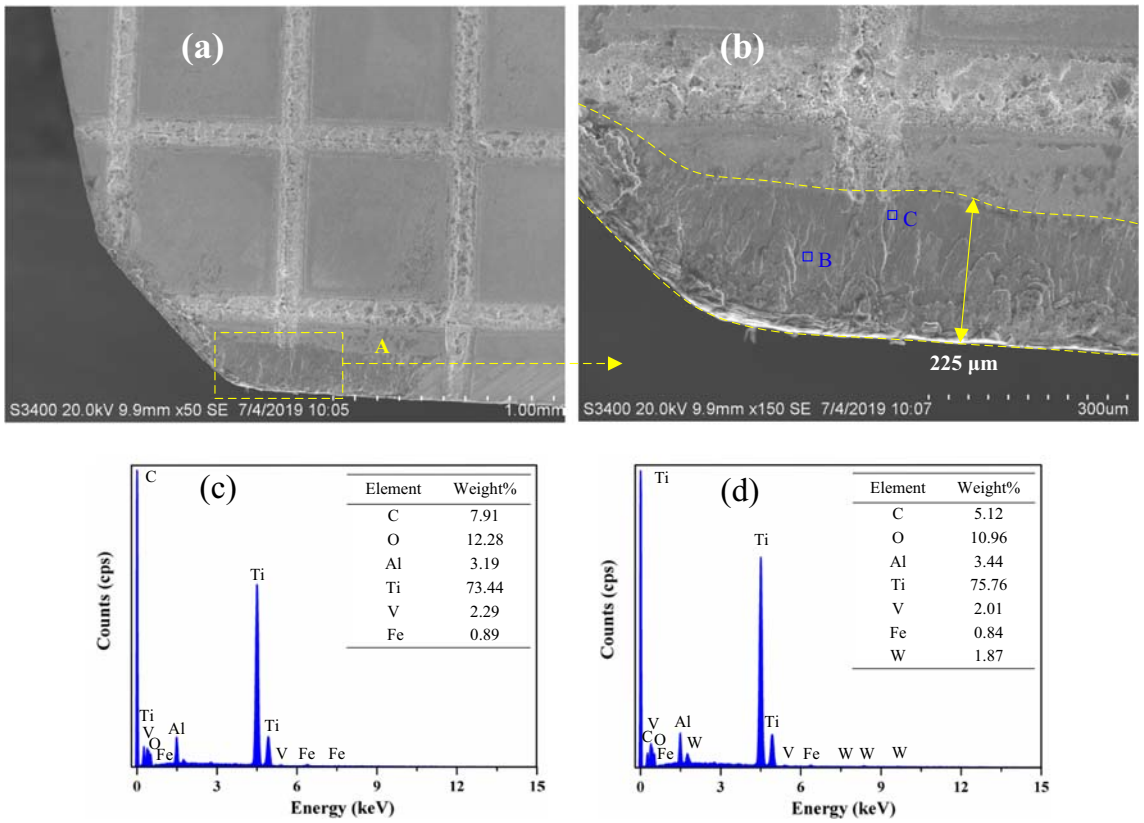

Fig. 16 SEM and EDX of the wear on the rake face of the rhombic-textured tool ($v = 90.4$ m/min, $a_p = 0.4$ mm): **b** enlarged view of A; **c** EDX of B; **d** EDX of C

The existence of a texture of the tool can effectively collect debris, reduce the retention of debris, and slow down the wear of a tool. In addition, the existence of a texture enlarges the heat dissipation area, reduces the

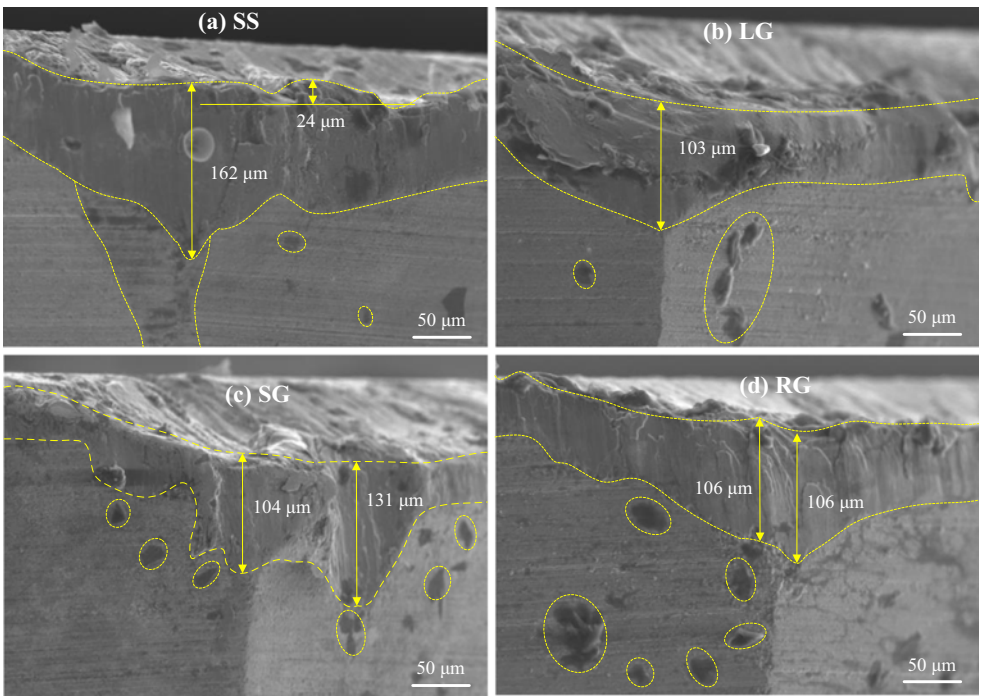

Fig. 17 SEM on the flank face of the four kinds of tools ($v = 90.4$ m/min, $a_p = 0.4$ mm)

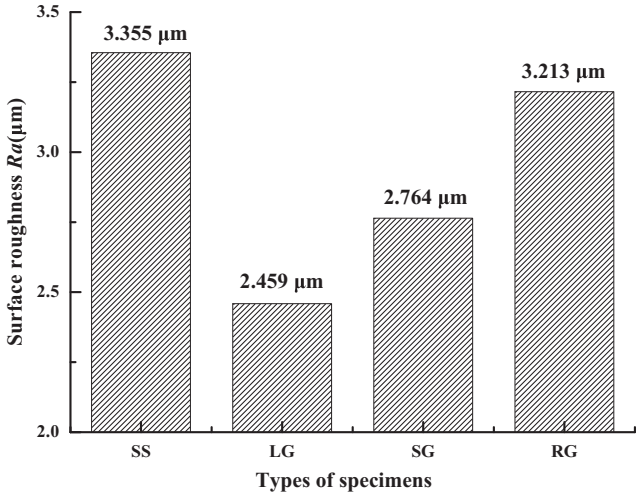

Fig. 18 Machined surface roughness of titanium alloy ($v = 90.4$ m/min, $a_p = 0.4$ mm)

cutting temperature, reduces the occurrence of oxidative wear of a tool, and improves the tool wear form. Texturing a tool improves the wear condition e and makes the wear area on the rake face smaller. Therefore, the friction coefficient is decreased. The friction coefficient of the textured YG8 tools is smaller than that of the non-textured YG8 tool, as shown in Figs. 8 and 9.

Compared with the textured YG8 tools, the non-textured YG8 tool is worn more seriously on the rake face, which forms crater wear near the main cutting edge. The main cutting edge becomes irregular because of the bonding effect of the titanium alloy. In Fig. 17a, showing the wear track of the non-textured tool, the wear accumulates near the main cutting edge to form a certain height, which will aggravate the wear on the flank face, so that the wear area of the flank face is much larger than that of the textured tools (Fig. 17b–d). The flank face of the tool comes in contact with the machined surface of the titanium alloy, and the wear of the non-textured tool is more serious than that of groove textured tools. Therefore, the surface of the titanium alloy machined by the non-textured tool is rougher.

5 Conclusions

Three kinds of rake-faced textures were machined on YG8 tool by laser processing equipment. Experiments were carried out in dry cutting titanium alloy. The wear mechanism of the tool, chip morphology, and bonding layer state were analyzed and discussed. Main conclusions were drawn as follows:

(1) The existence of micro texture on YG8 tool rake face can greatly reduce the cutting force of the cutting process, reduce the friction coefficient between the YG8 tool rake face and workpiece, improve the chip morphology, and slow down the wear of the tool.
(2) Among the three kinds of groove-textured tools, the line-textured tool has the best effect, compared with the sinusoidal- and rhombic-textured tools.
(3) Texture has a significant effect on the failure mode of a tool. Bond wear, oxidation wear, and diffusion wear occur simultaneously of the non-textured tool. Bond wear is the main wear mode for the line- and sinusoidal-textured tools, and oxidation wear is the main wear mode for the rhombic-textured tool.
(4) The existence of a texture reduces the tool-chip contact length and the contact area. Therefore, the texture reduced heat generation in the contact zone. The texture can collect debris and reduce the occurrence of abrasive wear in the tool–chip contact area. In addition, the existence of the micro texture enlarges the heat dissipation area, reduces the cutting temperature, reduces the occurrence of oxidative wear, and improves the tool wear form.

Acknowledgments The authors thank engineer Jingjie Dai for his great help with the SEM and associate professor Fulin Jiang for his great help in revising the article.

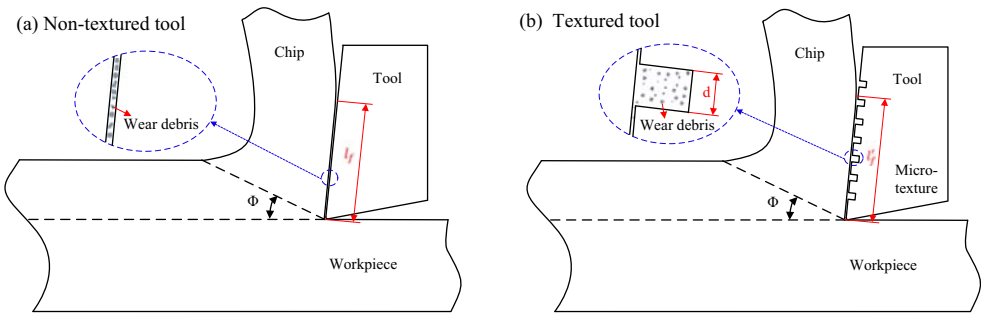

Fig. 19 Schematic diagram of cutting

Funding information This work is supported by the Natural Science Foundation of Shandong Province (ZR2018PEE011 and ZR2019MEE059), Key Research and Development Program of Shandong Province (2019GNC106102).

References

1. Weinert K, Inasaki I, Sutherland JW, Wakabayashi T (2004) Dry machining and minimum quantity lubrication. CIRP Ann Manuf Technol 53:511–537
2. Dong L, Li CH, Bai XF, Zhai MG, Qi Q, Yin QA, Lv XJ, Li LF (2019) Analysis of the cooling performance of Ti-6Al-4V in minimum quantity lubricant milling with different nanoparticles. Int J Adv Manuf Technol 103:2197–2206
3. Khalili NR, Duecker S, Ashton W, Chavez F (2015) From cleaner production to sustainable development: the role of academia. J Cleaner Production 96:30–43
4. Shokrani A, Dhokia V, Newman ST (2012) Environmentally conscious machining of difficult-to-machine materials with regard to cutting fluids. Int J Mach Tools Manuf 57:83–101
5. Sreejith PS, Ngoi BKA (2000) Dry machining: machining of the future. J Mater Process Technol 101:287–291
6. Zhou CC, Guo XH, Zhang KD, Cheng L, Wu YQ (2019) The coupling effect of micro-groove textures and nanofluids on cutting performance of uncoated cemented carbide tools in milling Ti-6Al-4V. J Mater Process Technol 271:36–45
7. Xie J, Luo MJ, Wu KK, Yang LF, Li DH (2013) Experimental study on cutting temperature and cutting force in dry turning of titanium alloy using a non-coated microgrooved tool. Int J Mach Tools Manuf 73:25–36
8. Xie HB, Wang ZJ (2019) Study of cutting forces using FE, ANOVA, and BPNN in elliptical vibration cutting of titanium alloy Ti-6Al-4V. Int J Adv Manuf Technol 105:5105–5120
9. Jiang F, Liu Z, Yang F, Zhong Z, Sun S (2018) Investigations on tool temperature with heat conduction and heat convection in high-speed slot milling of Ti6Al4V. Int J Adv Manuf Technol 96(5–8): 1847–1858
10. Priya R, Somashekhar SH (2019) Role of textured tool in improving machining performance: a review. J Manuf Process 43:47–73
11. Liu X, Liu Y, Li L, Tian Y (2019) Optimization of the micro-textures on the cutting tool based on the penetration of the lubricant in the micro-textures. Int J Adv Manuf Technol 104:3173–3180
12. Vasumathy D, Meena A (2017) Influence of micro scale textured tools on tribological properties at too-chip interface in turning AISI 316 austenitic stainless steel. Wear 376-377:1747–1758
13. Vamsi KP, Srikant RR, Nageswara RD (2010) Experimental investigation on the performance of nanoboric acid suspensions in SAE-40 and coconut oil during turning of AISI 1040 steel. Int J Mach Tools Manuf 50:911–916
14. Chang T, Guo ZW, Yuan CQ (2019) Study on influence of Koch snowflake surface texture on tribological performance for marine water-lubricated bearings. Tribol Int 129:29–37
15. Wieslaw C, Pawel P, Slawomir S, Waldemar K, Michal W (2018) Evolutions of cylinder liner surface texture and tribological performance of piston ring-liner assembly. Tribol Int 127:545–556
16. Song WL, Wang ZC, Wang SJ, Zhou K, Guo Z (2017) Experimental study on the cutting temperature of textured carbide tool embedded with graphite. Int J Adv Manuf Technol 93:3419–3427
17. Aizawa T, Mitsuo A, Yamamoto S, Sumitomo T, Muraishi S (2015) Self-lubrication mechanism via the in situ formed lubricious oxide tribofilm. Wear 259:708–718
18. Arulkirubakaran D, Senthilkumar V, Chilamwar VL, Senthil P (2019) Performance of surface textured tools during machining of Al-Cu/TiB_2 composite. Measurement. https://doi.org/10.1016/j.measurement.2019.02.013
19. Liu YY, Deng JX, Wang W, Duan R, Xing YQ (2019) Characterization of green Al_2O_3 ceramics surface machined by tools with textures on flank-face in dry turning. Int J Appl Ceram Technol. https://doi.org/10.1016/j.ceramint.2018.08.163
20. Hao XQ, Cui W, Li L, Li HL, Khan AM, He N (2018) Cutting performance of textured polycrystalline diamond tools with composite lyophilic/lyophobic wettabilities. J Mater Process Technol 260:1–8
21. Sanjib KR, Meinam AS, Deba KS (2018) A comparative study in machining of AISI D2 steel using textured and non-textured coated carbide tool at the flank face. J Manuf Process 36:360–372
22. Xing YQ, Deng JX, Zhao J, Zhang GD, Zhang KD (2014) Cutting performance and wear mechanism of nanoscale and microscale textured ceramic tool in dry cutting of hardened steel. Int J Refract Met Hard Mater 43:46–58
23. Orra K, Choudhury SK (2018) Tribological aspects of various geometrically shaped micro-textures on cutting insert to improve tool life in hard turning process. J Manuf Process 31:502–513
24. Chen YD, Guo XH, Zhang KD, Guo DL, Zhou CC, Cai LW (2019) Study on the surface quality of CFRP machined by micro-textured milling tools. J Manuf Process 37:114–123
25. Mishra SK, Ghosh S, Aravindan S (2019) Performance of laser processed carbide tools for machining of Ti6Al4V alloys: a combined study on experimental and finite element analysis. Precis Eng 56:370–385
26. Li N, Chen YJ, Kong DD, Tan SL (2017) Experimental investigation with respect to the performance of deep submillimeter-scaled textured tools in dry turning titanium alloy Ti-6Al-4V. Appl Surf Sci 403:187–199
27. Arulkirubakaran D, Senthilkumar V, Kumawat V (2016) Effect of micro-textured tools on machining of Ti-6Al-4V alloy: an experimental and numerical approach. Int J Refract Met Hard Mater 54: 165–177
28. Xing YQ, Deng JX, Zhao J, Zhang GD, Zhang KD (2014) Cutting performance and wear mechanism of nanoscale and microscale textured Al_2O_3/TiC ceramic tools in dry cutting of hardened steel. Int J Refract Met Hard Mater 43:46–58
29. Wu Z, Deng JX, Su C, Luo C, Xia D (2014) Performance of the micro-texture self-lubricating and pulsating heat pipe self-cooling tools in dry cutting process. Int J Refract Met Hard Mater 45:238–248
30. Sugihara T, Enomoto T (2017) Performance of cutting tools with dimple textured surfaces: a comparative study of different texture patterns. Precis Eng 49:52–60
31. Xing YQ, Deng JX, Li SP, Yue HZ, Meng R, Gao P (2014) Cutting performance and wear characteristics of Al_2O_3/TiC ceramic cutting tools with WS_2/Zr soft-coatings and nano-textures in dry cutting. Wear 318:12–26
32. Kawasegi N, Sugimori H, Morimoto H, Morita N, Hori L (2009) Development of cutting tools with microscale and nanoscale textures to improve frictional behavior. Precis Eng 33:248–254
33. Lei S, Devarajan S, Chang Z (2009) A study of micro-pool lubricated cutting tool in machining of mild steel. J Mater Process Technol 209:1612–1620